ELSEVIER

Contents lists available at ScienceDirect

Journal of Magnetism and Magnetic Materials

journal homepage: www.elsevier.com/locate/jmmm





First-principles calculations of the high-pressure behavior, electronic, magnetic, and elastic properties of praseodymium pnictides: PrX (X = P, As and Bi)

T. Ghellab ^{a,b}, H. Baaziz ^{a,b,*}, Z. Charifi ^{a,b}, H. Latelli ^{a,b}, Mais Jamil A. Ahmad ^{c,d}, Mahmoud Telfah ^e, Ahmad Alsaad ^e, Ahmad Telfah ^c, Roland Hergenröder ^c, Renat Sabirianov ^f

- ^a Department of Physics, Faculty of Science, University of M'sila, 28000 M'sila, Algeria
- ^b Laboratory of Physics and Chemistry of Materials, University of M'sila, Algeria
- ^c Leibniz Institut für Analytische Wissenschaften-ISAS-e.V., Bunsen-Kirchhoff-Straße 11, 44139 Dortmund, Germany
- ^d Institut für FestkörperphysikTechnische Universität Berlin, Hardenbergstraβe 36, Berlin 10623, Germany
- e Department of Physical Sciences, Jordan University of Science & Technology, P.O. Box 3030, Irbid 22110, Jordan
- f Department of Physics, University of Nebraska at Omaha, Omaha, NE 68182, USA

ARTICLE INFO

Keywords: Rare earths Electronic properties Elastic properties Hubbard Magnetic moment Mechanical stability

ABSTRACT

We report ab-initio calculation of the structural, magnetic, elastic, and electronic properties of the PrX (X = P, As and Bi). The structural stability and phase transition of PrX (X = P, As, Bi) compounds in (NaCl-type), (CsCl-type), (Zinc blende-type), WC-Bh (Hexagonal) and L10 (Tetragonal) structures in ferromagnetic state are investigated using the augmented plane wave plus local orbital (APW + lo) method within GGA + U, and mBJ-GGA + U approximations. Careful inspection of electronic properties indicates that most of the compounds exhibit half-metallic behavior. The total magnetic moment of all investigated compounds is obtained to be 2 μ B. The mechanical stability test performed on the computed elastic constants Cij demonstrate that investigated compounds are mechanically stable. To elucidate chemical stability, chemical bonds are investigated and found to be mainly characterized by an ionic-covalent mixture. Moreover, elastic anisotropy of all compounds is calculated. Subsequently.

1. Introduction

The rare earth functional materials have attracted much attention owing to their outstanding magnetic, structural, electronic and optical properties. Much effort has been paid to elucidate their physical properties as well as their technological applications [1–7]. Because of their distinctive magnetic, phosphorescent, and catalytic characteristics, rare earth materials have become highly essential in our world of technology. These elements are essential in a wide range of technology, from cell phones and televisions to LED light bulbs and wind turbines in spintronics and spin filtering devices. The categorization of rare earths and their compounds in terms of their valences gives an elementary understanding of their physical characteristics while also generating a wide range of magnetic structures. Changes in the rare earths lattice parameter in particular may be correlated with the valence charge. The pressure–volume connection has reveal that Yb pnictide compounds, like

europium chalcogenides, undergo a pressure induced structural phase change from *NaCl* (B1)- to the *CsCl* (B2). They found no abnormalities in the compression curves of these compounds, which have been seen in most intermediate valence compounds and are caused by a change in valence state [8]. Experimentally, such materials can be epitaxially grown on III-V semiconductors [9].

The occurrence of unfilled f-electron shells of lanthanide pnictinides, which is highly delocalized and hence strongly interacting with the lattice [8], has associated most of these unusual properties. These materials have been demonstrated to be epitaxially grown on III–V semiconductors [9].

Praseodymium chalcogenides are technologically attractive because of their potential applications in hyperfine enhanced nuclear magnetic cooling allowing the use of these compounds in electronic devices such as metal-based transistors [7] as well as in spin filtering devices and in spintronic. A comprehensive study of the electronic and magnetic

^{*} Corresponding author at: Department of Physics, Faculty of Science, University of M'sila, 28000 M'sila, Algeria. E-mail address: baaziz_hakim@yahoo.fr (H. Baaziz).

structure as well as the structural and elastic properties presents an important platform for the systematic understanding and development of the lanthanide and actinide mono-pnictide.

Synchrotron X-ray diffraction study of the mono-pnictides PrX (X = P, As, Sb, Bi) and CeX (X = P, As, Sb, Bi), Shirotani et al. [10–12] and Adachi et al. [13] reveal a cubic NaCl (B1)-type phase at room temperature and ambient pressure. At high pressure, monopnictides undergoe a phase transition from NaCl (B1)- to the CsCl (B2)-type structure.

A phase transition of *PrP* [13] from the cubic B1 to the tetragonal B2 structure at a pressure of 26 GPa inducing a volume reduction of 12.1% has been reported. Other family compounds such as *PrBi* [10], *PrSb* [11] and *PrAs* [12] undergo a phase transition at pressures of 14, 13 and 27 GPa, respectively. This is similar to praseodymium chalcogenide, such as *PrTe* compound, where the existence of a single crystallographic phase transition from B1 to B2 occurs at a pressure of 9.1 GPa resulting in a volume reduction of 11.5% [14] that has been experimentally confirmed.

The treatment of the degree of localization of 4*f* electrons represents a considerable challenge. The appropriate determination of the electronic properties of rare earth compounds is therefore an engaging issue. In order to provide a basic explanation of the physical properties of rare earths, a correlation between the valence electrons and the properties of these compounds must be developed. Particularly, the change of the number of valence electrons directly influences the change of the lattice parameter [15]. By employing the *Muffin-Tin* linear orbital method using the atomic sphere approximation with an exchange and correlation potential calculated by the local density approximation, De et al. was able to calculate the electronic properties of praseodymium pnictides [6].

Under high pressure, the application of the inter-ionic potential theory allowed Pagare et al. [16] to compute the structural properties of LnAs (Ln = Ce, Pr, Nd and Sm) compounds. Using the local spin density approximation (LDA), the electronic properties of praseodymium monopnictides and monochalcogenides have been reported by Vaitheeswaran et al. [5]. In order to study the elastic and structural properties of PrY: Y = P, As, Sb, Bi and PrX: X = S, Se, Te, Soni et al. employed the inter-ionic potential theory taking into account the off-electron Coulomb screen effect [7]. First principles calculations have been reported for the electronic structure of RX (R = Ce, Pr, Nd, Pm, Sm, Eu, Gd, Tb, Dy, Ho, Er, Tm, Yb, Lu; X = N, P, As, Sb, Bi, S, Se, Te) by Petit et al. [3]. In addition, ab-initio results were reported for the vibrational, elastic and structural properties of PrS. PrSe and PrTe were calculated [17].

In this work, we report *ab-initio* findings of the structural, elastic, electronic and magnetic properties of PrP, PrAs and PrBi. The hydrostatic-pressure induced phase transitions for each of the investigated compounds is presented. The band structure as well as the total and partial density of states are analyzed. Finally, magnetic properties as well as elastic constants.. We computed and then displayed the anisotropic Young's modulus three-dimensional stereograms. For more details on the elastic anisotropy of PrX (X = P, As and Bi) we have plotted the cross sections in the (X = Y), (XY), (XZ) and (YZ) crystal planes of the 3D surface of Young's modulus (E).

2. Calculation details

Augmented Plane wave plus local orbital method (APW + lo) implemented in the wien2k code is utilized to calculate physical properties of PrX (X = P, As, Bi) [18]. The PBE exchange and correlation potential is handled within generalized gradient approximation (GGA) [19]. No approximation of the shape of the potential is made as the cutoff potential extends to 12. The cut-off for the plane wave density is set to $K_{max} = 8.5/R_{MT}$. For all phases, $R_{M.T}$ is chosen between 2.1 and 2.4 atomic units (a.u.) for Pr, P, As and Bi atoms. Based on the model of Monkhorst and Pack [20], an 18*18*18 grid of k points was chosen to allow integration in their reducible part of the $Brillouin\ Zone$. When the

charge difference is less than 1 mRy, convergence is achieved. For accurate calculation of the bandgap energy, the mBJ approach is employed [21].

The description of localized electronic states such as the d and f states is inadequate when using the GGA approximation. For compounds whose electrons are strongly correlated, modelling of exchange and correlation interactions within the framework of DFT lacks accuracy. Therefore, errors in the description of physical properties are expected. This inaccuracy is attributed to the lack of discontinuity in the derivative of the exchange–correlation function with respect to the electron occupancy number [22–25].

For the treatment of strongly correlated electrons and based on the Hubbard model approach, the DFT + U approach aims at eliminating the self-interaction error and also corrects the standard GGA exchange correlation by spatially introducing the on-site Coulomb interaction in localized narrow bands. Therefore, for real systems, if one wants the GGA + U approximation to yield improvements over the GGA, the choice of the Hubbard parameter U is the key. We used the scheme introduced by Anisimov et al. [26] and Gunnarsson et al. [27].

The Slater transition rule [28] allows the following equation to be obtained,

$$U_{eff} = \begin{cases} \varepsilon_{3d\uparrow} \left[n_{3d\uparrow} = \frac{n}{2} + \frac{1}{2}, n_{3d\downarrow} = \frac{n}{2} \right] - \varepsilon_{3d\downarrow} \left[n_{3d\uparrow} = \frac{n}{2} + \frac{1}{2}, n_{3d\downarrow} = \frac{n}{2} - 1 \right] \\ -\varepsilon_F \left[n_{3d\uparrow} = \frac{n}{2} + \frac{1}{2}, n_{3d\downarrow} = \frac{n}{2} \right] + \varepsilon_F \left[n_{3d\uparrow} = \frac{n}{2} + \frac{1}{2}, n_{3d\downarrow} = \frac{n}{2} - 1 \right] \end{cases}$$

$$(1)$$

where $\varepsilon_{3d\uparrow}$ and $\varepsilon_{3d\downarrow}$ are the 3d eigenvalues at the central atom calculated at the fixed occupancies. In the case of praseodymium, we used Eq. (1), but for the orbitale 4f rather than the orbitale 3d. In Ref. [29], we argue that we should use this value for U_{eff} and set J to zero. The calculated values of U_{eff} are: U(Pr)=2.95787 eV for $PrP_{,}$ U(Pr)=3.05309 eV for PrAs and U(Pr)=2.94241 eV for PrBi.

3. The crystal structure and phase stability study of PrX compounds (X = P, As and Bi)

The PrX (X=P, As and Bi) compounds crystalize in the following structures: B1 (NaCl-type), B2 (CsCl-type), B3 (Zinc blende-type), WC-Bh (Hexagonal) and L1 $_0$ (Tetragonal) with space groups $Fm\overline{3}m$ (225), $Pm\overline{3}m$ (221), $F\overline{4}3m$ (216), $P\overline{6}2m$ (187), and P4/mmm (123), respectively with the Wyckoff atomic positions:

B1: Pr(0, 0, 0) and X(1/2, 1/2, 1/2), B2: Pr(0, 0, 0) and X(1/2, 1/2, 1/2), B3: Pr(0, 0, 0) and X(1/4, 1/4, 1/4) $\alpha = \beta = \gamma = 60^{\circ}$, WC-Bh: Pr(0, 0, 0) and X(2/3, 1/3, 1/2), L1₀: Pr(0, 0, 0) and X(1/2, 1/2, 1/2) (see Fig. 1).

To determine the equilibrium parameters such as the lattice parameter (a_0) , the modulus of compressibility B and its derivative B', the total energy of PrX (X = P, As and Bi) compounds in all structures (B1, B2, B3, WC-Bh and L1₀) was calculated from first principles as a function of volume using GGA in the ferromagnetic phase. The curve obtained was fitted to the Murnaghan equation [30].

Fig. 2 clearly indicates that the most stable phase in all compounds is the B1 phase (halite, commonly known as rock salt, NaCl type). The B3 phase remains an unstable phase for the three PrX (X = P, As and Bi) compounds. Table 1 indicates an increase of the equilibrium lattice parameter upon changing the atom X = P, As, Bi, respectively, in accordance with the atomic radius increasing from phosphorus to arsenic to bismuth atoms. For the lattice parameter and the compressibility modulus in all phases, a good agreement with previous theoretical and experimental results is observed despite which atom X = P, As, Bi is substituted.

The Pr in B1 phase is coordinated by six equivalent X atoms (and vice versa) to form a mixture of corner and edge-sharing PrX_6 octahedra. The

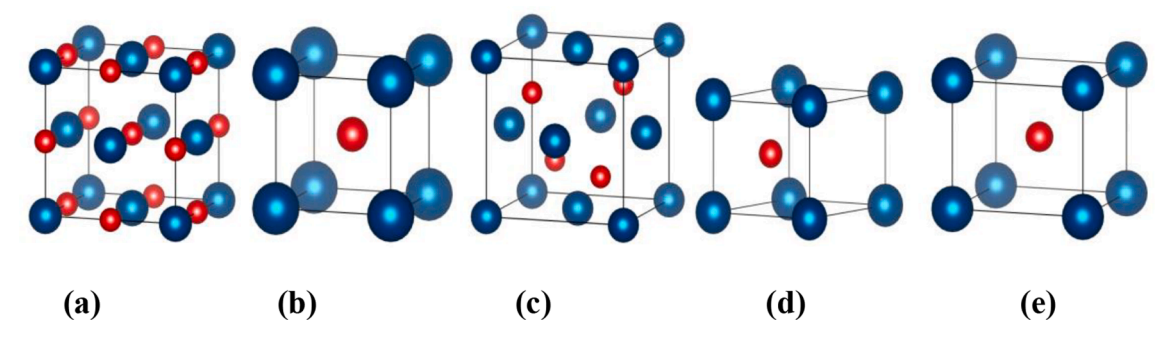


Fig. 1. The crystal structure of. **(a)** B1 (Cubic *NaCl*), **(b)** B2 (Cubic *CsCl*), **(c)** B3 (Cubic Zinc blende), **(d)** WC-Bh (Hexagonal), **(e)** L1₀ (Tetragonal) of the compounds *PrX* (*X* = *P*, *As* and *Bi*). *Pr*. blue, *X*. red.

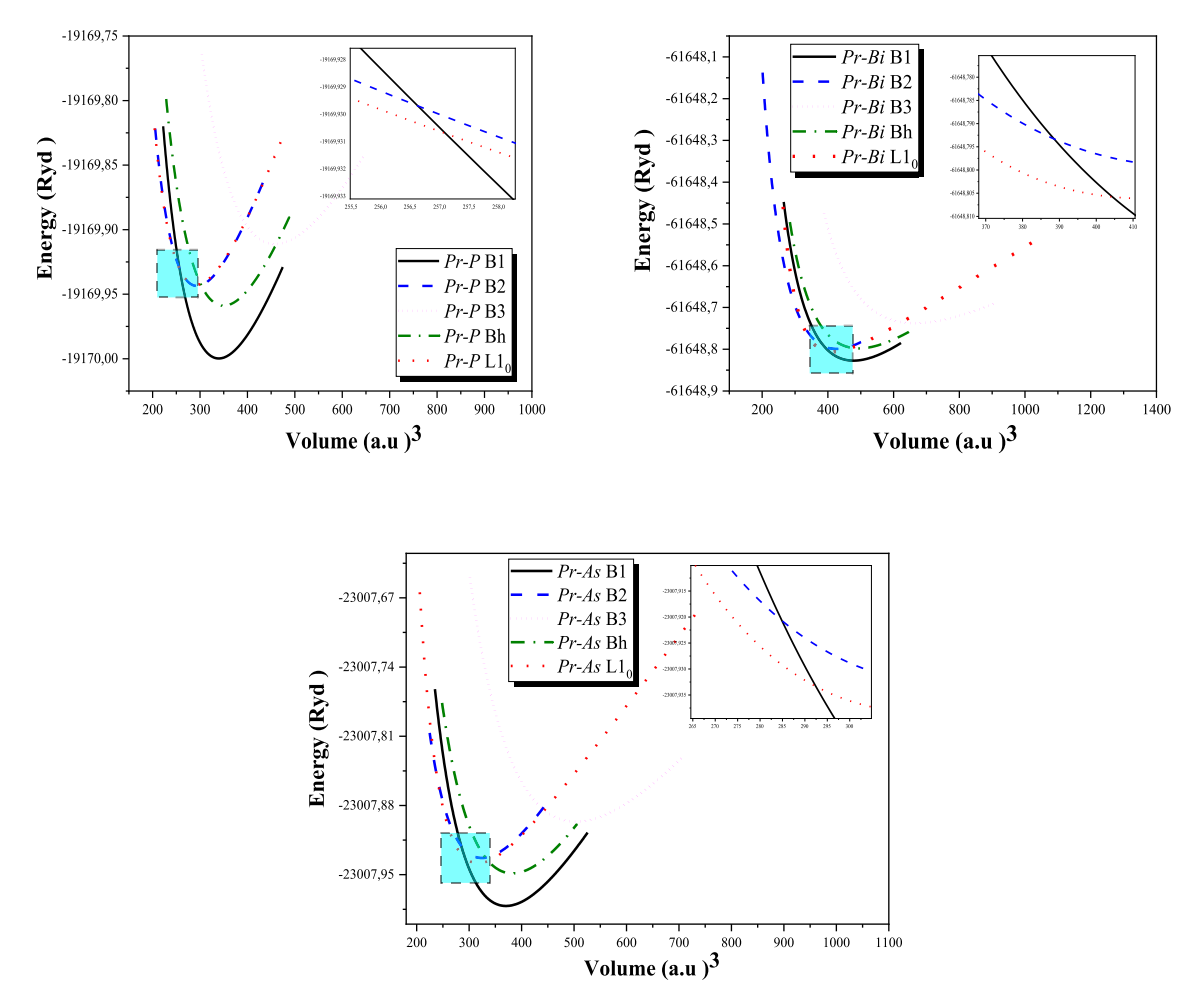


Fig. 2. The variation of energy versus volume of PrX(X = P, As and Bi) compounds in all crystal structures calculated using GGA method.

corner-sharing octahedral are untilted. The Pr-P, Pr-As and Pr-Bi bond lengths are 2.9496 Å, 3.01240 Å and, 3.015 Å respectively (see Fig. 3).

Two different methods are used to calculate the transition pressure. It is accurate calculation is necessary to determine the stability of a phase. Theoretical details are already shown in previous works [35,36]. The first method is based on the calculation of the tangent, from the E(V) curves, between the difference in energy and the difference in volume. The second method is based on Gibbs energy calculations. Since theoretical calculations are performed at 0 K, free energy becomes equal to the enthalpy (*H*). Consequently, phases with the lowest enthalpy are stable phases and the transition pressure is determined when the enthalpies of both phases are equal.

As pressure elevated, a phase transition from B1 to B2 phase, followed and a transition from B2 to $L1_0$ phase for the *PrX* (X = P, As and Bi) (see Fig. 4).

Using both methods we found that there are two phase transitions. The first is a phase transition from the more stable B1 phase to a metastable L1₀ phase when applying a pressure of 20.75 GPa, 13.37 GPa and 6.04 GPa (second method) for the compounds *PrP*, *PrAs* and *PrBi* respectively. Another phase transition occurs when the pressure is increased and we will have a second phase transition from a stable phase B1 to another metastable phase B2 when a pressure of 22.03 GPa, 18.28 GPa and 8.85 GPa (second method) is applied for the compounds *PrP*, *PrAs* and *PrBi* respectively. It can be concluded that the coexisting

Table 1 Structural properties of PrX. The lattice constants a, c in Å and c/a, the modulus of compressibility B (GPa), its derivative B' and the minimum total energy E_{min} (Ryd) calculated by GGA.

Compounds	Phases	Theoretical and experimental work	The lattice	e constants		B (GPa)	B'	E_{min} (Ryd)
			a (Å)	c (Å)	c/a			
PrP	B1	Present	5.860			64.217	3.718	-19170
		Theory [31]	5.950			75.218	3.768	
		Theory [5]	5.890			70		
		Theory [6]	5.905					
		Theory [7]	5.897			75.1	5.11	
		Experimental [8]	5.872			74 ± 2		
		Experimental [1]	5.893					
		Experimental [32]	5.905					
	B2	Present	3.518			68.102	4.327	-19169.944
		Theory [31]	3.623			74.072	3.709	
	В3	Present	6.476			43.156	3.524	-19169.911
		Theory [31]	6.553			48.639	3.775	
	WC-Bh	Present	4.013	3.602	0.897	58.702	3.355	-19169.959
		Theory [31]	4.042	3.741	0.925	68.459	3.420	
	$L1_0$	Present	3.712	4.509	1.214	66.367	4.499	-19169.943
		Theory [31]	4.632	3.918	0.846	78.164	3.637	
PrAs	B1	Present	6.032			57.820	3.962	-23007.981
		Theory [31]	6.094			67.457	3.768	
		Theory [5]	6.048			64		
		Theory [6]	6.030					
		Theory [7]	6.02			89.9 100 ± 7	$5.3\ 4.5{\pm}0.6$	
		Experimental [8]	6.009					
		Experimental [10]	6.018					
		Experimental [32]	6.030			59.651	4.401	
	B2	Present	3.636			66.645	3.784	-23007.896
		Theory [31]	3.724			38.455	3.602	
	В3	Present	6.683			43.65	3.789	-23007.896
		Theory [31]	6.735			55.091	3.453	
	WC-Bh	Present	4.135	3.807	0.920	62.022	3.592	-23007.948
		Theory [31]	4.146	3.834	0.926	66.630	6.577	
	$L1_0$	Present	3.785	4.567	1.206	68.103	3.961	-23007.939
		Theory [31]	4.756	4.089	0.860			
PrBi	B1	Present	6.567			42.642	3.766	-61648.827
		Theory [33]	6.566			48.940 51	4.227	
		Theory [5]	6.424					
		Theory [6]	6.461			$42.51\ 40\pm5$		
		Theory [34]	6.383				5.14	
		Experimental [10]	6.455			46.736	13 ± 6	
		Experimental [1]	6.461			49.234		
	B2	Present	3.981			25.751	3.555	-61648.799
		Theory [33]	4.018			30.254	3.884	
	В3	Present	7.332			37.602	3.906	-61648.738
		Theory [33]	7.329			45.086	4.023	222.21700
	WC-Bh	Present	4.496	3.959	0.880	47.740	3.858	-61648.798
	110 Dii	Theory [33]	4.472	4.159	0.930	52.108	4.064	010 10.7 70
	L1 ₀	Present	4.085	3.339	0.930	32.100	6.639	-61648.806
	F10	Theory [33]	5.139	4.62	0.890		4.065	010 10.000

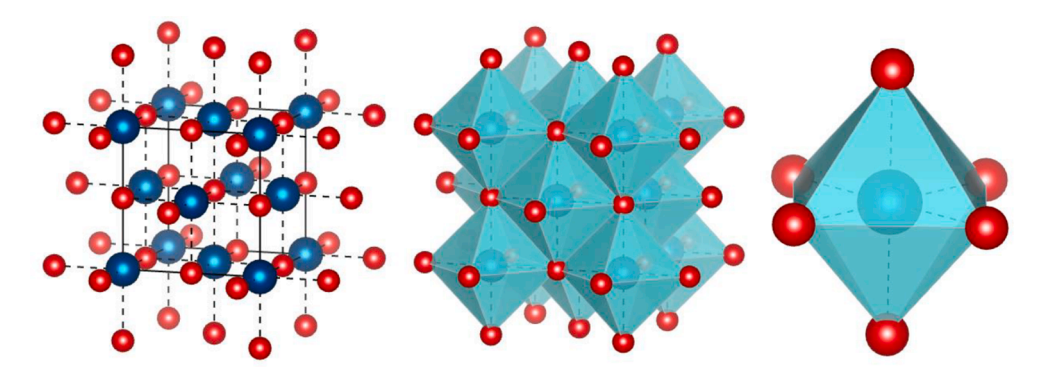


Fig. 3. The crystallographic representation of the most stable ferromagnetic phase B1 with octahedral sites of PrX (X = P, As and Bi). Pr. Blue color, X = P, As and Bi. Red color.

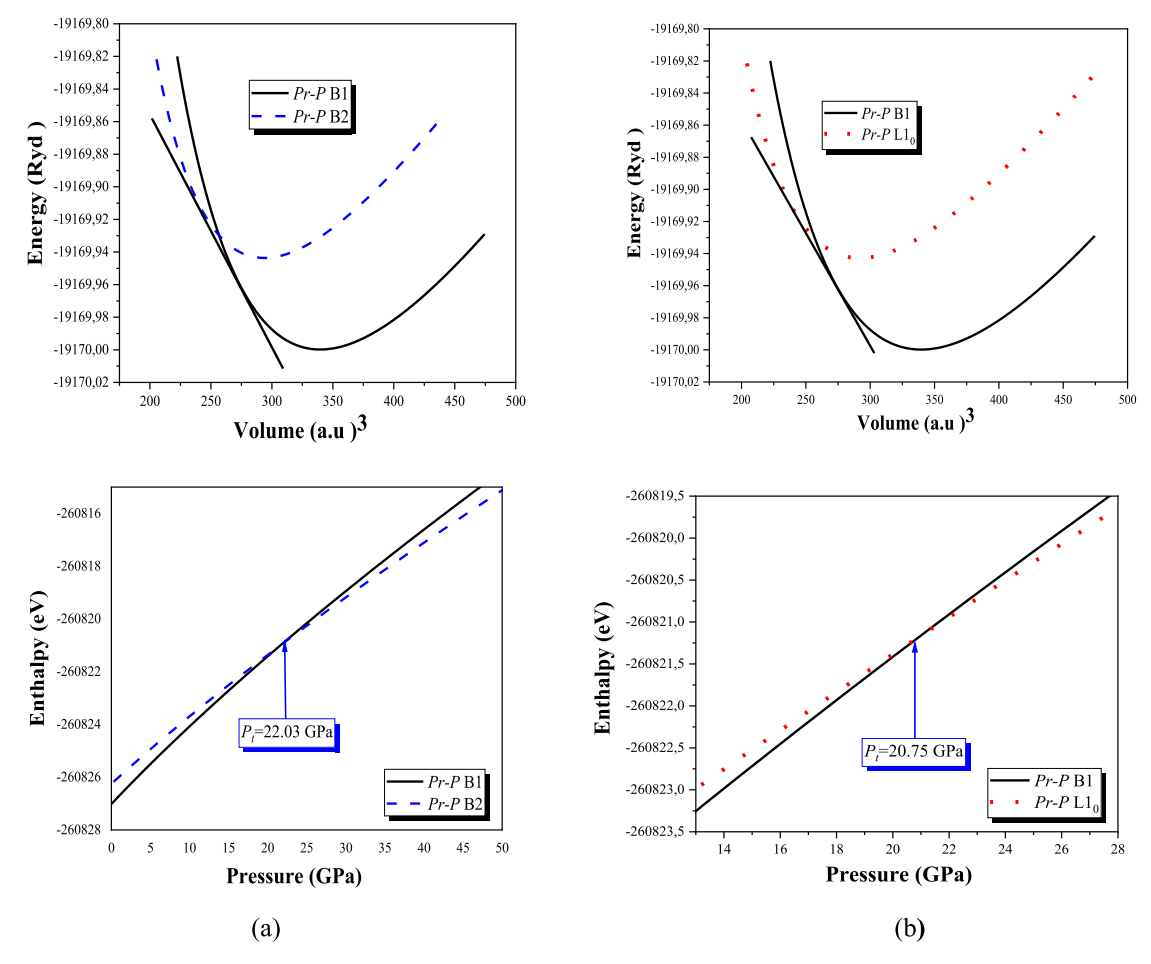


Fig. 4. Variation of total energies as a function of volume and variation of total enthalpies as a function pressure of unit cell. B1 phase (Black-solid curve), B2 (Bluedashed curve), and L1₀ phase (Red-dot curve) using GGA for. (a) and (b) *PrP* compound, (c) and (d) *PrAs* compound, (e) and (f) *PrBi* compound.

conditions of the metastable phase $L1_0$ is very peculiar because, using the second method, it exists for a pressure range of 20.75–22.03 GPa, 13.37–18.28 GPa and 6.04–8.85 GPa for the compounds *PrP*, *PrAs* and *PrBi* respectively. So a small perturbation can affect the stability conditions of these compounds.

Second method reveals phase transition from B1 to B2 occurs at transition pressures of 22.03, 18.28 and 8.85 GPa (see Table 2) for PrX (X = P, As and Bi), respectively. For both PrP and PrAs, these values are smaller than the experimental values (26 and 27 GPa) of Shirotani et al. [10]. However, relative error found from the experiment is smaller than found theoretically (16 and 26 GPa) of Vaitheeswaran et al. [5]. For PrP and PrAs, a phase transition from B1 to $L1_0$ was also detected which has not been reported yet in previous work. This transition occurs at transition pressures of 20.75 and 13.37 GPa for PrP and PrAs, respectively. The obtained results indicate that second method is more accurate than the first method as the relative error found is smaller than the experimental ones.

4. Electronic and magnetic properties

To elucidate chemical bonding in a material, it is important to understand band structures and densities of states. We used the structural parameters previously found using the GGA and GGA + U approximations for the most stable phase (B1 phase). The band structure of PrX (X = P, As and Bi) compounds is calculated using the GGA, GGA + U, mBJ and mBJ-GGA + U approximations along the main symmetry directions of the first $Brillion\ Zone$ (see Fig. 5).

Using GGA approximation for the PrP and PrAs compounds indicates the absence of the energy gap for the majority spins (up) and minority spins (down) cases. On the other hand, using GGA + U, mBJ-GGA and mBJ-GGA + U approximations for the minority spins (down), Fermi level crosses the conduction band that is shifted downwards demonstrating the existence of an indirect energy gap (F-X). However, majority spins are characterized by a metallic character. Moreover, FPP and FP-FP compounds are found to be almost half-metals or one can say non-ideal half-metals.

By using GGA (GGA + U) or mBJ (mBJ-GGA + U) approximation for the PrBi compound, for the minority spins (down), the Fermi level is observed to be located between the conduction band and the valence band revealing the existence of an indirect energy gap (Γ -X). On contrary, for the majority spins, we notice the absence of the energy gap and thus PrBi compound is a half metal. Table 3 shows that the values of energy gap decrease for the PrP to PrAs to PrBi sequence.

Density of states investigation reveals that major contribution to the valence bands of Pr monopnictides comes from p-band and d-states of the ligand and partially constituted by the f-bands of Pr. In addition, for all monopnictides, valence band is completely separated from the conduction band around the Γ point. The f-bands of Pr are completely separated from the Δ band and dip below the bands of the p-states at the X level in PrX. This overlap increases as the sequence goes from Bi to As to P and there is a very small gap at the X point in PrBi. Moving from PrP to PrAs to PrBi, the BV width of f-states decreases from 21.7 mRyd to 14.4 mRyd [37]. Moving down, the pnictogen column has an increase in lattice constant leading to an increase in Pr-Pr separation and hence the

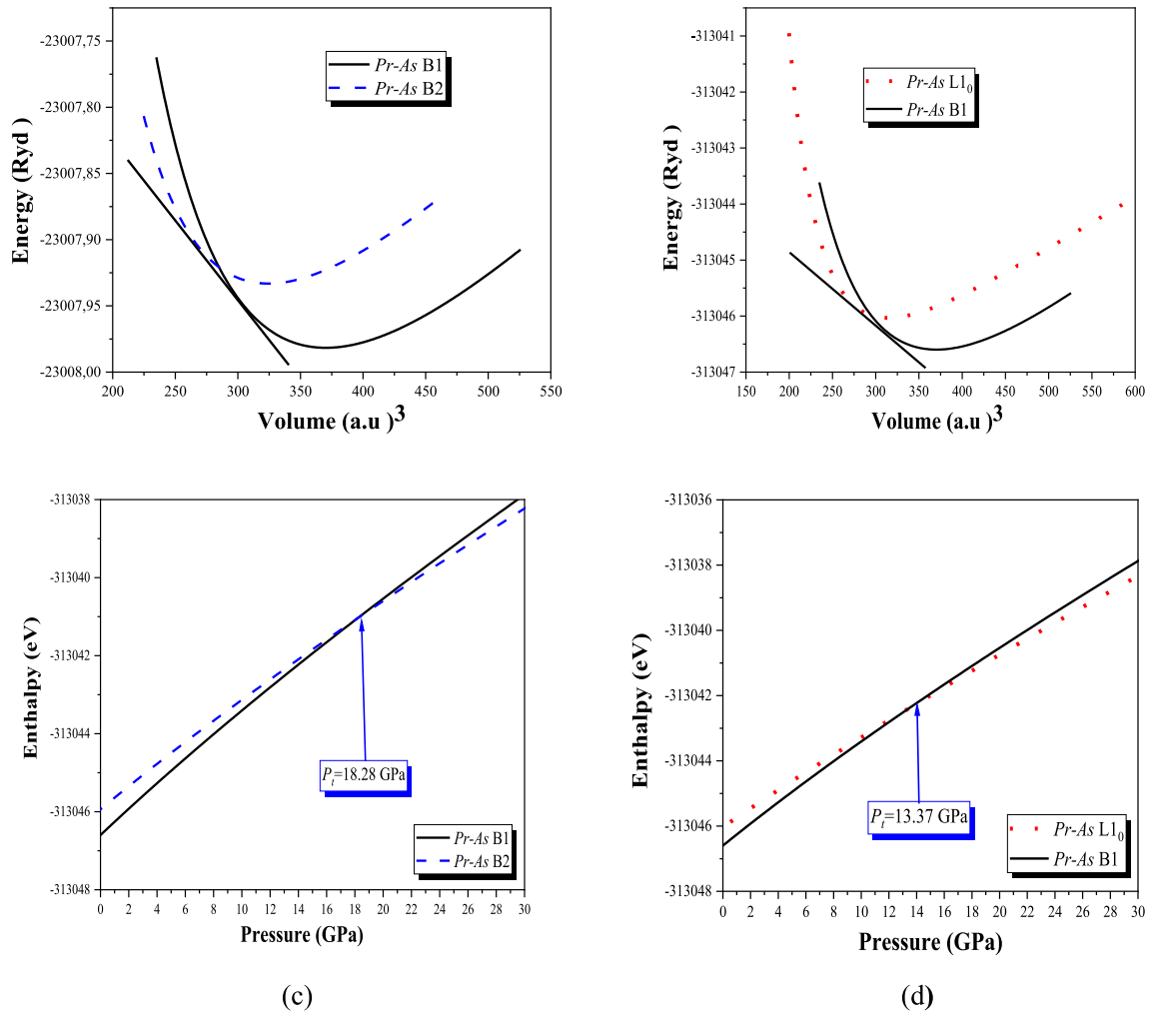


Fig. 4. (continued).

bandwidth of -f decreases.

The representation of the total and partial densities of state of PrX (X = P, As and Bi) is given in Fig. 6. The parts of the bands between (-12 eV and -8 eV) (VB1) are mainly dominated by the contribution of the s orbital of X for both spins. The part between (-4 eV and E_F), for both up and down spins show a weak intensity dominated mainly by the p-orbital contribution of X. Examination of the conduction band between (E_F and S eV) (CB1) indicates that these bands are mainly composed of the f orbital of the Pr atom. Furthermore, the major contribution to the conduction band between (S eV and S eV) (CB2) comes from the S orbital of the S ratio.

The DOS highlights the presence of a huge peak around the *Fermi* energy, which is a common feature of all compounds. This peak comes from the f-bands. For the majority spins and for all pnictogens, we noticed the existence of three peaks for the occupied part of the DOS. Additionally, examining Fig. 6 bellow E_F shows the appearance of the first peak that can be attributed to the f-states of Pr. The main contributions to the second and third peaks come from the p-states of pnictogen. In addition, under E_F the first three peaks are separated by a sharp minimum. Moving down the pnictogen column, we notice that the positions of the pnictogen p-state peaks remain invariant while the height decreases and consequently the width increases. The conduction band consists mainly of the d states of Pr and the width of this band decreases as the atomic number of the pnictogen increases.

The values of the total DOS at E_F , $N(E_F)$ up and down for the PrX (X = P, As, Bi) compounds are presented in Table 4. Using GGA

approximation, as the pnictogen changes from P to Bi, $N(E_F)$, increases from 35.89 to 116.44 states/Ryd as the DOS of the f states at E_F increases from 35.8 to 65.92 states/Ryd. Thus, the hybridization of the band states increases as $N(E_F)$ increases. The DOS of p-states of X decrease from 2.85 to 1.83 as the pnictogen changes from Bi to P.

The total magnetic moment as well as those of Pr, P, As and Bi atoms. Table 5 reports the magnetic moments m_0 (μ_B /f. u) calculated for PrX (X = P, As, Bi) using the GGA, GGA + U, mBJ and mBJ-GGA + U approximations. The total magnetic moment is found to be 2 μ B for the PrX (X = P, As, Bi) compounds. It can be seen from Table 5 that the contribution of the Pr atom is much larger than that of the X atom at the Fermi level. As a result, X atom has approximately no effect on the total magnetic moment.

5. Elastic properties

The mechanical and dynamic behavior of solids can be linked through the elastic constants. In addition, elastic constants provide an additional insight on the nature of the forces operating in crystals, rigidity, and stability of crystalline solids. It is known that forces as well as elastic constants can be represented by first and second order functions of potentials. For their *ab initio* calculations, accurate methods should be employed. In particular, the accuracy of the calculation of forces acting in solids must be verified. From the known crystal structures of the materials, an *ab-initio* modelling bias allows us to obtain elastic data that can be calculated using two frequently used methods [38–41]. The first

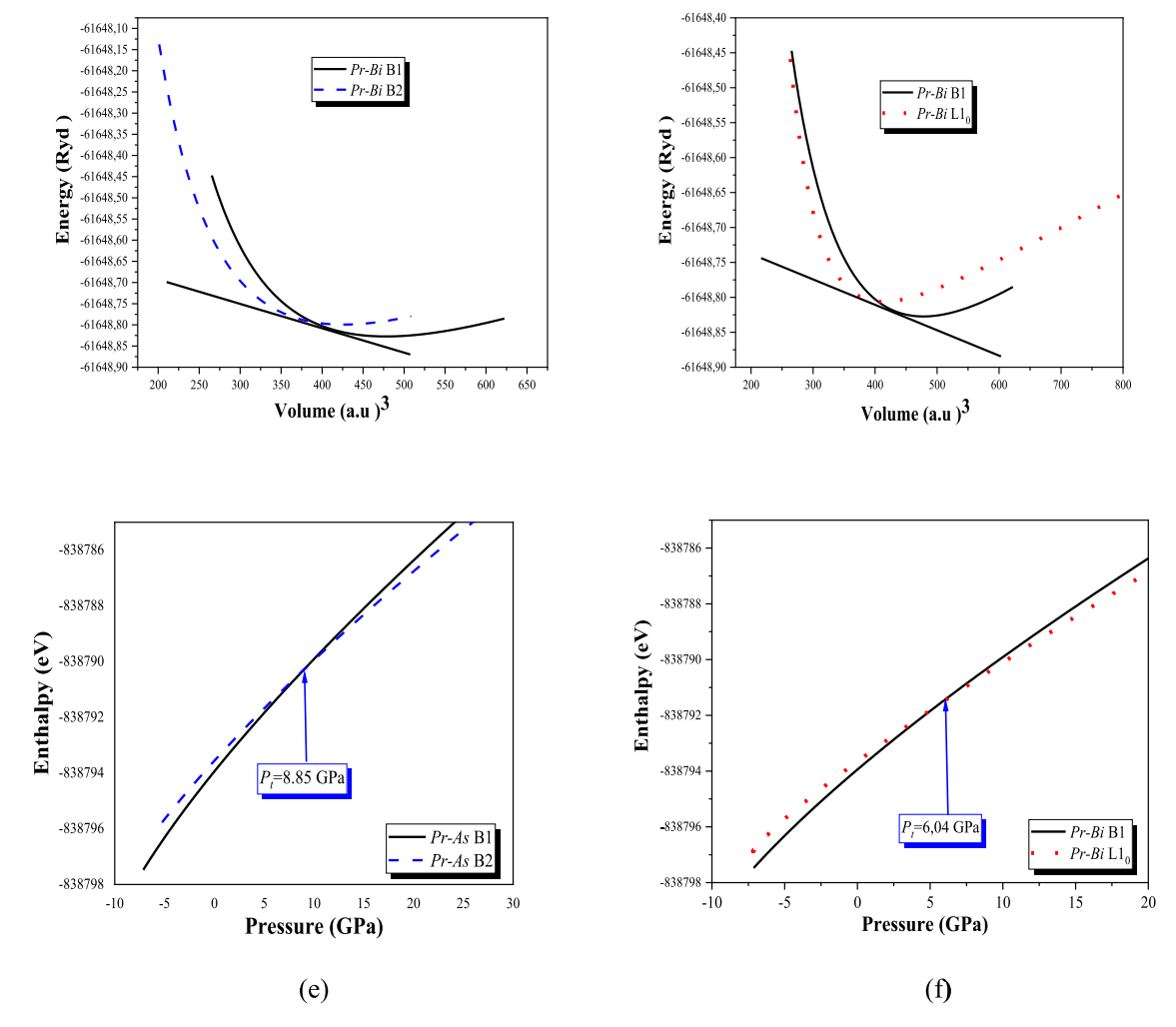


Fig. 4. (continued).

Table 2 The phase transition pressure (Pt) in GPa calculated with both methods for the compounds PrX (X = P, As and Bi).

Compounds	Phase transitions	Our Pt (GPa) calculations		Other Pt (GPa) calculations	
		1st method	2nd method		
PrP	B1 → B2	17.74	22.03	EXP :26 [7], Theo : 16 [5], 25 [7], 36 [31]	
	$B1 \rightarrow L1_0$	13.62	20.75		
PrAs	$B1 \to B2$	15.48	18.28	EXP: 27 [8], 26 [12], Theo: 12 [5], 26 [7], 30 [31]	
	$B1 \rightarrow L1_0$	12.80	13.37		
PrBi	$B1 \rightarrow B2$	8.1	8.85	Theo: 16 [33], 8 [5]	
	$B1 \rightarrow L1_0$	5.30	6.04	EXP: 14 [12], Theo: 14.4 [33]	

method is the stress—strain method where an analysis of changes in stress values leading to changes in strain is made. The second method is called the volume conservation technique that is based on the analysis of the total energy of the deformed states of the material.

In order to obtain the elastic constants C_{ij} , we employ the stress–strain method. The values of C_{ij} are collected in Table 6. Our findings indicate that calculations executed are reasonable compared to previous theoretical data. Furthermore, stability criteria indicate that compounds investigated are mechanically stable as they satisfy the following conditions: $C_{11} > 0$, $C_{11} - C_{12} > 0$, $C_{44} > 0$, $C_{11} + 2C_{12} > 0$ and $C_{12} < B > C_{11}$.

Therefore, B1 phase of PrX (X = P, As, Bi) is mechanically stable. Cauchy relation [42] can describe the characterization of non-central forces in solids. In a cubic system this relation is given by C_{12} - $C_{44} = 2P$ [43] where P is the Cauchy pressure. If the Cauchy pressure is negative, the materials have a directional bonding character. If the Cauchy pressure is positive, the materials have a metallic bonding character. In this work C_{12} - C_{44} are negative. As a result, PrX compounds have directional bonds with angular character. Indeed, the negative Cauchy pressure observed for the most stable phase of the PrX (X = P, As and Bi) compounds probably comes from electronic transitions.

Table 6 demonstrates that the value of C_{II} is greater than the other constants, so we can say that PrX compounds have a greater resistance to length change than the resistances to shape and volume change. It is deduced that the $\langle 100 \rangle$ directions are the densest.

The most important elastic properties from the technological point of view are the bulk's modulus, the Young's modulus E and the Poisson's ratio σ . The three parameters can be calculated using the following equations [44]:

$$\sigma = \frac{1}{2} \frac{\left(B_H - \frac{2}{3}G_H\right)}{B_H + \frac{1}{2}G_H} \tag{2}$$

where $G_H = \frac{1}{2}(G_V + G_R)$ is the isotropic shear modulus, G_V is Voigt's shear modulus and G_R is Reuss's shear modulus and can be written as [45–47]: $G_V = \frac{1}{5}(C_{11} - C_{12} + 3C_{44})$, $G_R = \frac{5(C_{11} - C_{12})C_{44}}{4C_{44} + 3(C_{11} - C_{12})}$ and $B_H = (C_{11} + 2C_{12})/3$.

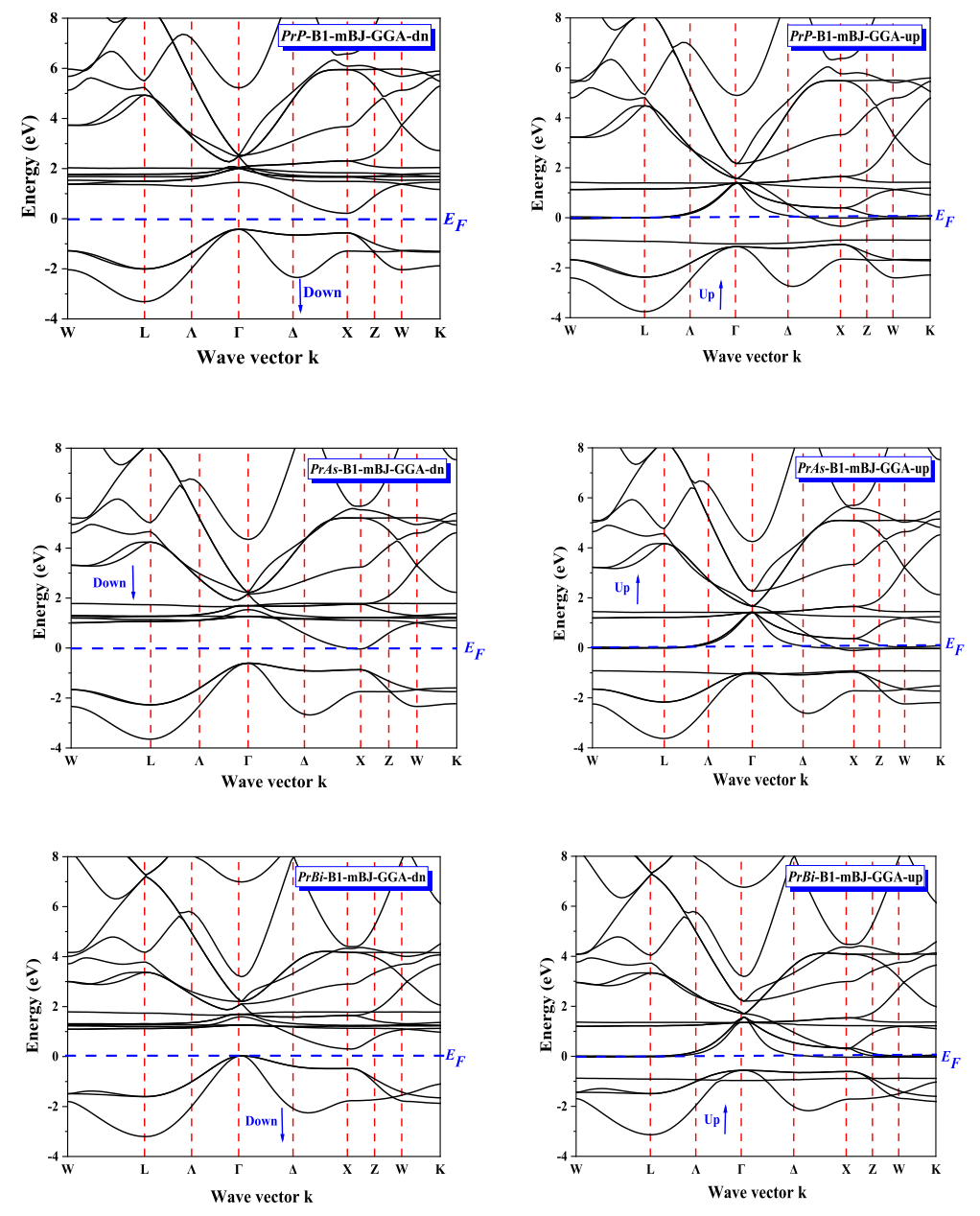


Fig. 5. Band structure along the symmetry lines of the *Brillouin Zone* for PrX (X = P, As and Bi).

Table 3 The energy gap values (eV) calculated with the GGA, GGA + U, mBJ-GGA and mBJ-GGA + U approximations for the PrX (X = P, As and Bi) compounds.

	and of the approximations for the first (if			1) 110 and 21) compounds.		
Gap	Approximations		PrP	PrAs	PrBi	
Eg (eV)	GGA	Dn	/	/	0.189	
		Up	/	/	/	
	GGA + U	Dn	0.35	0.3	0.19	
		Up	/	/	/	
	mBJ-GGA	Dn	0.7	0.621	0.30	
		Up	/	/	/	
	mBJ- $GGA + U$	Dn	0.65	0.59	0.40	
		Up	/	/	/	

Table 7 compares the compressibility moduli calculated from *Cij* with those obtained from the EOS equations of state for the same materials. An excellent agreement between the *B* values calculated using the GGA method. This correspondence between the *B* values calculated from the *Cij* and those calculated from the *EOS* gives a general idea of the

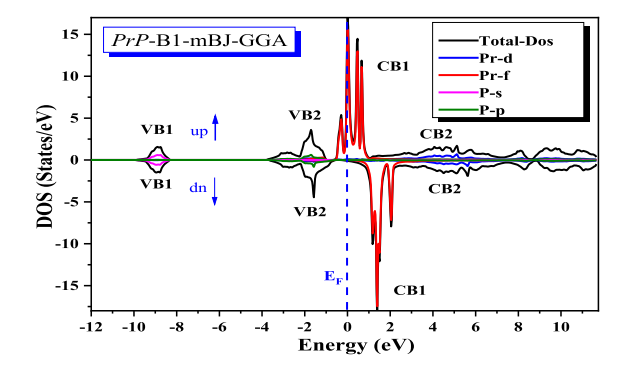
reliability of our Cij calculations.

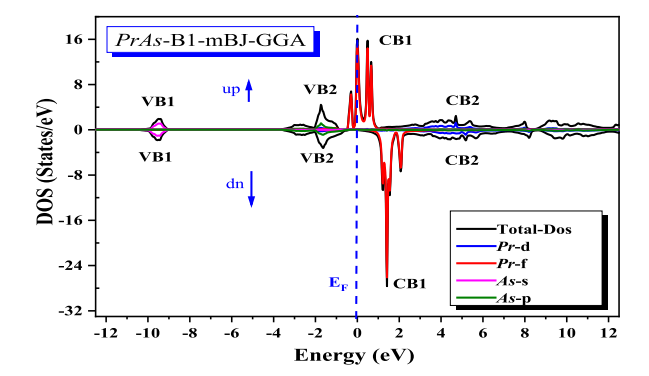
The modulus of compressibility of *PrP* is greater than that of *PrAs* and *PrBi*, indicating that the bonding in *PrP* is stronger than that of *PrAs* and *PrPi*.

The Poisson's ratio σ , Young's modulus E, isotropic shear modulus G and B/G for PrX (X=P, As and Bi) are presented in Table 7. The obtained mechanical parameters are in good agreement to those obtained in previous theoretical works [31–33]. To elucidate the nature and strength of the bond forces, Poisson's ratio is calculated. It is value is limited between 0.25 and 0.5 for central forces in solids [48]. The calculated values of σ are equal to 0.228, 0.238 and 0.240 for PrX (X=P, As and Bi), respectively. The obtained σ is less than 0.25 indicating that the forces are not totally central. In other words, an ionic-covalent mixture characterizes chemical bonds of the three compounds.

In order to gain further insight into the stiffness measurement of solids, it is important to calculate the Young's modulus *E*. It increases in the ascending order, *PrBi* to *PrAs* to *PrP*. Thus, *PrP* is the stiffest.

The measure of resistance to volume change when an external





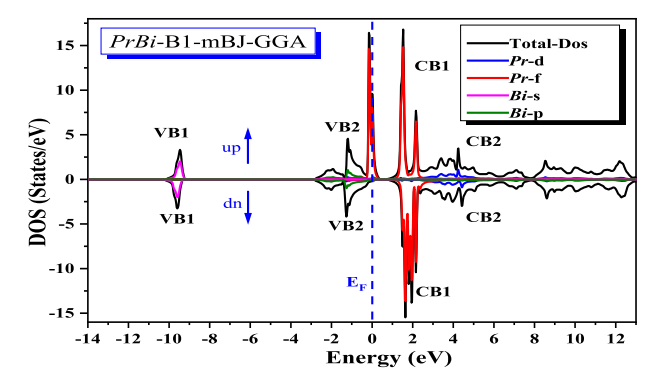


Fig. 6. The calculated total and partial density of states of PrX (X = P, As and Bi). The graph is scaled for 0 eV at the Fermi level (E_F).

pressure is applied is manifested by the modulus of compressibility. The resistance to reversible deformation under shear stress [49] can be represented by the shear modulus. Therefore, by using the isotropic shear modulus, the hardness of a material can be determined more accurately than by using the compressibility modulus. The hardness of the three compounds increases as we go from *PrBi* to *PrAs* to *PrP* implying that *PrBi* is softer than the other two compounds. This is consistent with the results extracted from Young's modulus.

For polycrystalline phases, the ratio of the compressibility modulus

to the shear modulus B/G is calculated considering that the compressibility modulus B represents the resistance to rupture while the shear modulus G represents the resistance to plastic deformation. A low (high) B/G ratio is an indication of brittleness (ductility). Ductile materials are separated from brittle materials by a critical value of about 1.75. The calculated values of the B/G ratios are 1.51. 1.57 and 1.59 for PPP, PPAS and PPBI, respectively indicating that the three compounds are brittle.

Several physical properties such as melting temperature and specific heat are closely related to the Debye temperature θ_D . At low temperatures, θ_D obtained from the elastic constants is the same as that obtained from the specific heat measurements. This is because at low temperatures, vibrational excitations come from acoustic vibrations only. We used the calculated elastic constants and average sound velocity ν_m to calculate the Debye temperature θ_D [50],

Table 5 The theoretical values of the magnetic moment m_0 (μ_B /f: u) calculated for PPP, PPAs and PPBi by the GGA, GGA + U, mBJ-GGA and mBJ-GGA + U approximations.

Compounds	Approximations	The moment m_0 (μ_B /f. u)				
		Total	Interstitial	Pr	X	
PrP	GGA	1.96976	0.13701	1.88078	-0.04803	
	mBJ-GGA	1.99423	0.11843	1.90998	-0.03417	
	GGA + U	2.00953	0.08467	1.98527	-0.06041	
	mBJ-GGA + U	2.01467	-0.12356	2.25641	-0.11818	
PrAs	GGA	1.99318	0.09738	1.96352	-0.06772	
	mBJ-GGA	1.99973	0.06125	1.98045	-0.04196	
	GGA + U	2.05475	0.04373	2.09847	-0.08744	
	mBJ-GGA + U	2.04821	-0.02394	2.17169	-0.09954	
PrBi	GGA	2.02825	0.14706	1.93673	-0.05553	
	mBJ-GGA	2.04447	0.10203	1.99924	-0.05680	
	GGA + U	2.17923	0.11182	2.14106	-0.07365	
	mBJ-GGA + U	2.29032	-0.00854	2.41834	-0.11949	

Table 6 The elastic constants for PrX (X = P, As and Bi) calculated using GGA and Zener anisotropy factor A.

Compounds	PrP		PrAs		PrBi	
	Our results	DFT	Our results	DFT	Our results	DFT
C ₁₁ (GPA)	180.2	183.4 [31] 156.78 [7]	171.28	169.1 [31] 191.88 [7]	125.7	128.29 [33] 103.22 [7]
C ₁₂ (GPA)	23.5	25.0 [31] 34.34 [7]	20.6	21.25 [31] 38.97 [7]	13.2	13.11 [33] 20.32 [7]
C ₄₄ (GPA)	36.9	37.8 [31] 34.54 [7]	31.40	32.14 [31] 39.23 [7]	21.3	17.37 [33] 20.58
Α	0.471	0.477 [31]	0.416	0.435 [31]	0.378	0.302

Table 4 The total electron density $N(E_F)$ up and down at the *Fermi* level using the GGA, GGA + U, mBJ-GGA and mBJ-GGA + U approximations with *P* polarization for the *PrP*, *PrAs* and *PrBi* compounds.

Approximations	PrP	PrP			PrAs			PrBi		
	$N(E_F)$		P $N(E_F)$		P	$N(E_F)$		P		
	$N(E_F)\uparrow$	$N(E_F)\downarrow$		$N(E_F)\uparrow$	$N(E_F)\downarrow$		$N(E_F)\uparrow$	$N(E_F)\downarrow$		
GGA	35.89	0.84	95.42%	100.42	2.42	95.29%	116.44	9.62	84.73%	
GGA + U	49.62	0.7	97.21%	116.33	2.28	96.15%	127.95	4.77	92.81%	
mBJ-GGA	68.17	0	100%	350.61	0.11	99.93%	352.30	0.61	99.65%	
mBJ- $GGA + U$	61.03	0	100%	472.38	0.64	99.72%	486.29	1.84	99.24%	

Table 7 Elasticity modulus B_V , B_R , B_H , G_V , G_R , G_H , E_V , E_R , E_H , σ_V , σ_R , σ_H , B_H/G_H , A_B %, A_G % and A^U for PrP, PrAs and PrBi by the GGA.

Compounds	PrP	PrAs	PrBi
B_V (GPA)	75.7333	70.8267	50.7
B_R (GPA)	75.7333	70.8267	50.7
B_H (GPA)	75.7333	70.8267	50.7
G_V (GPA)	53.48	48.976	35.28
G_R (GPA)	46.8045	40.9542	28.3446
G_H (GPA)	50.1423	44.9651	31.8123
	51.1 [31]	45.2 [31]	28.78 [33]
E_V (GPA)	129.87	119.405	85.9124
E_R (GPA)	116.429	103.008	71.6765
E_H (GPA)	123.23	111.335	78.9286
	125 [31]	110.84 [31]	72.195 [33]
σ_V	0.214194	0.21902	0.217579
σ_R	0.243775	0.257605	0.264377
σ_H	0.228807	0.238012	0.240537
	0.223 [31]	0.226 [31]	0.254 [33]
B_H/G_H	1.51037	1.57515	1.59372
A_B %	0	0	0
A_G %	6.65654	8.92008	10.9006
$A^{\widetilde{U}}$	0.713124	0.979368	1.22341

$$\theta_D = \frac{h}{k_B} \left(\frac{3n}{4\pi} \left(\frac{N_a \, \rho}{M} \right) \right)^{\frac{1}{3}} v_m \tag{3}$$

where h is Planck's constant, k_B is Boltzmann's constant, N_a is the Avogadro number, ρ is the density of the molecule, M is the molecular weight, and n is the number of atoms in the molecule. The average velocity ν_m of polycrystalline materials is given by [51],

$$v_m = \left(\frac{1}{3} \left(\frac{2}{v_t^3} + \frac{1}{v_l^3}\right)\right)^{-\frac{1}{3}} \tag{4}$$

where v_t and v_t are longitudinal and transverse elastic velocities that can be obtained from the Navier equation [52],

$$v_{l} = \left(\frac{3B + 4G}{3\rho}\right)^{\frac{1}{2}} \quad \text{and} \quad v_{t} = \left(\frac{G}{\rho}\right)^{\frac{1}{2}}$$
 (5)

The values of v_l , v_t , v_m and θ_D calculated at zero pressure using GGA for *PrP*, *PrAs* and *PrBi* are presented in Table 8. Evidently, elastic compressional waves (longitudinal waves) propagate faster than the elastic shear waves (transverse waves).

The θ_D parameter is calculated to be 342.303 K, 291.699 K and 197.946 K for PrX (X=P, As and Bi), respectively. Its value is higher than that of the constituent atom Pr (153 K). The melting temperatures are found to be 1311.32 \pm 300 K and 1265.69 \pm 300 K for PrX (X=P, As). These values are significantly higher than that of Pr atom (1205 K). On the other hand, PrBi is found to exhibit a melting temperature of 1078.51 \pm 300 K that is lower than that of Pr atom.

The degree of elastic anisotropy has been calculated using different methods. It has already been calculated for other materials in previous

Table 8 The longitudinal, transverse, average elastic wave velocities, $(v_b, v_b, v_m \text{ in m/s})$, Debye temperature θ_D and melting temperature (in K) for *PrP*, *PrAs* and *PrBi* by the GGA.

Compounds	v_t (m/s)	ν _l (m/s)	ν _m (m/s)	θ _D (K)	Melting Temperature
PrP	3041.6	5129.14	3368.54	342.303	1311.32 ± 300 1636 ± 300 [31]
PrAs	2665.24	4545.37	2954.81	291.699	1265.69 ± 300 1552 ± 300 [31]
PrBi	1968.46 3260.65 [33]	3367.76 1872.06 [33]	2182.96 2079.3 [33]	197.946 118.8 [33]	1078.51 ± 300 1311 ± 300 [33]

works [53,54]. In this work we employed four different methods to estimate the elastic anisotropy for PrX (X = P, As and Bi). The first method is based on the calculation of the shear anisotropy factor that is given by the following expression for a cubic system.

$$A = \frac{2C_{44}}{C_{11} - C_{12}} \tag{6}$$

We can also measure the degree of elastic anisotropy in materials by calculating the Zener anisotropy factor A [44]. When this factor is equal to one for a given material, it is considered isotropic whereas if this factor differs from 1, the material is anisotropic. For PrX (X = P, As and Bi) compounds, Zener anisotropy factors are found to be 0.471, 0.416 and 0.378, respectively. Therefore, the three compounds are totally anisotropic (see Table 6).

The percentage of anisotropy in either shear (A_G) , or compression (A_B) are calculated by [55],

$$\begin{cases} A_B = (B_V - B_R)/(B_V + B_R) \times 100 \\ A_G = (G_V - G_R)/(G_V + G_R) \times 100 \end{cases}$$
 (7)

The constants A_G % = A_B % = 0 for isotropic materials. If their values deviate from 0 for a given material, it has some degree of anisotropy in either shear or compression.

Inspecting Table 7, $A_B=0$ for the three compounds confirming their isotropic nature in compression. Using GGA method, we calculate A_G % constant and found to be equal to 6.656, 8.920 and 10.900 for PrP, As and Bi, respectively. Our results confirm that PrBi is more anisotropic in shear than the other two compounds.

The third method is based on calculating universal index A^U given by [56].

$$A^{U} = \left(5\left(\frac{G_{V}}{G_{R}}\right) + \left(\frac{B_{V}}{B_{R}}\right)\right) - 6\tag{8}$$

If $A^U=0$, the compounds are isotropic. If A^U deviates from zero, A certain degree of elastic anisotropy is expected. Table 7 summarizes the results of the third method. Using the GGA approximation, $A^U=0.713$, 0.979 and 1.223 for PrP, PrAs and PrBi, respectively. Accordingly, all compounds show some degree of anisotropy. Furthermore, PrBi is predicted to be more anisotropic than the other two compounds.

The last method is based on the representation of E modulus distribution in 3D polar diagrams. For a cubic system [57],

$$E = \frac{1}{S_{11} - 2\left(S_{11} - S_{12} - \frac{1}{2}S_{44}\right)\left(n_1^2 n_2^2 + n_2^2 n_3^2 + n_3^2 n_1^2\right)}$$
(9)

 S_{ij} are the deformability elastic constants, $n_1 = sin\theta cos\phi$, $n_2 = sin\theta sin\phi$, and $n_3 = cos\theta$ are the directional cosines in spherical coordinates along x, y and z-axes.

A material is said to be completely isotropic if only the 3D shape of the Young's modulus is spherical. Otherwise, it is anisotropic and the degree of elastic anisotropy increases as the 3d surface is deformed. Fig. 7. (a) Shows that the surface of E is far from being spherical. It is completely deformed indicating a significant degree of anisotropy for PrP, PrAs and PrBi compounds. To obtain a further insight into the elastic anisotropy of PrX (X = P, As and Bi), we plotted the cross sections in the (X = Y), (XY), (XZ) and (YZ) crystal planes of the 3D surface of Young's modulus (E) (see Fig. 7 (b)). The plots demonstrate that elastic anisotropy in the (X = Y) plane is less important than in the (XY), (XZ), (YZ) planes. This confirms that compounds are more isotropic in the (X = Y) plane. In other planes, they exhibit more anisotropic behavior in Young's modulus.

For the compound PrP, the maximum value of Young's modulus is found for the [1 0 0] direction E(PrP) = 174.25 GPa and the minimum value is found for the [1 1 0] direction, E(PrP) = 60.67 GPa. In the case of PrAs: The maximum value of Young's modulus is calculated for the [1 0 0] direction, E(PrAs) = 166.85 GPa and the minimum value is

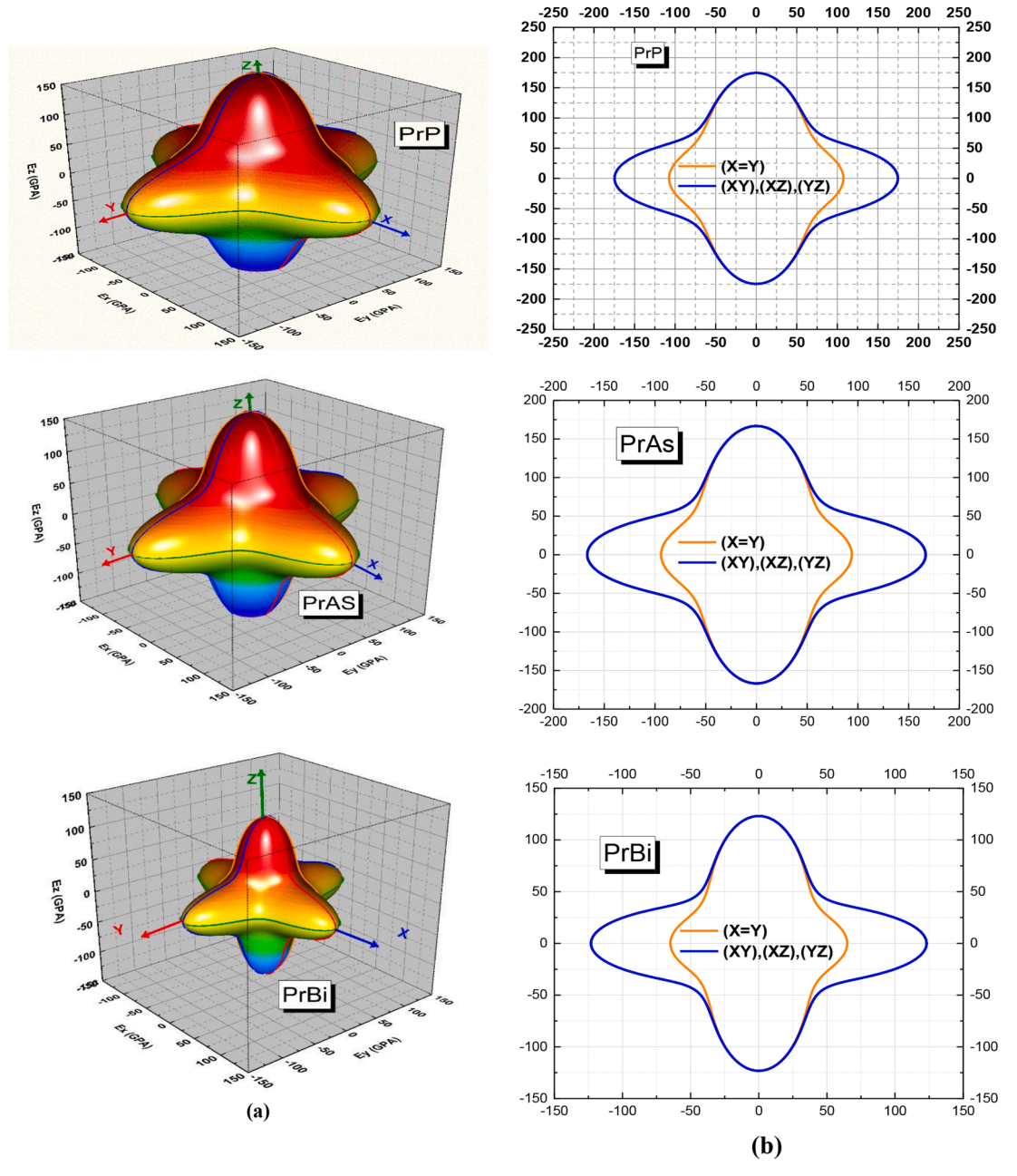


Fig. 7. The 3D surface of the Young's modulus (a) PrP, PrAs and PrBi (b) their cross section in the (X = Y) and (XZ), (XY), (YZ) planes.

obtained for the [1 1 0] direction, E(PrAs) = 52.31 GPa. For PrBi and for the [1 0 0] direction, E(PrBi) = 123.19 GPa is the maximum value of Young's modulus. The minimum value is obtained for the [1 1 0] direction, E(PrBi) = 34.21 GPa (see Fig. 7. (b)).

The disparity in Young's modulus between the maximum and minimum values is roughly 34.81 %, 31.35%, and 27.77% for *PrP*, *PrAs*, and *PrBi*, respectively. As a result, the three compounds are stiffer in the [1 1 0] direction with *PrP* being stiffer than the other two compounds.

6. Conclusion

We investigate the structural phase transition of $PrX\ (X = P, As, Bi)$ compounds in B1 (NaCl-type), B2 (CsCl-type), B3 (Zinc blende-type), WC-Bh (Hexagonal), and L10 (Tetragonal) structures in ferromagnetic state using the plane wave plus local orbital APW + lo method within the framework of density functional theory DFT. The exchange–correlation effects are treated using GGA and GGA + U approximations. The most

stable phase of PrX (X = P, As, Bi) compounds is the B1 phase (NaCl type). It undergoes a phase transition to the B2 and L1₀ phase under the effect of hydrostatic pressure. The B3 phase (Zinc-blende type) is an unstable phase. For PrP and PrAs, a phase transition from B1 to L1₀ is detected that has not been reported previously.

The GGA (GGA + U) and mBJ-GGA (mBJ-GGA + U) approximations are used for the calculation of electronic properties in the most stable phase B1. The compounds PrP and PrAs are predicted to be metals in the GGA approximation. However, other approximations predict both compounds to be half-metals. They behave as metals for the majority spins and semiconductors for minority spins characterized by the existence of an indirect energy gap (Γ -X). The four used approximations predict that PrBi is a half metal. The DOS curves obtained are almost similar for the PrX (X = P, As, Bi) compounds. The contribution of the Pr atom (the f-orbital) is the majority at the Fermi level.

GGA based calculations indicate that, as pnictogen P is replaced by Bi, $N(E_F)$, increases from 35.89 to 116.44 states/Ryd and the DOS of f-

states at E_F increases from 35.8 to 65.92 states/Ryd. Consequently, the hybridization of the band states increases as $N(E_F)$ increases. The DOS of p-states of X decreases from 2.85 to 1.83 as the pnictogen Bi replaced by P. The total magnetic moment of the three compounds is found to be 2 μ B. X atom has no effect on the total magnetic moment.

To elucidate mechanical properties, elastic constants C_{ii} , are calculated. Mechanical stability criteria indicate that the three compounds are mechanically stable. The modulus of compressibility of PrP is calculated to be greater than that of PrAs and PrBi compounds indicating that the bonding in PrP is stronger than that of PrAs and PrBi. The calculated values of Poisson's ratio σ are calculated to be 0.228, 0.238 and 0.240 for PrX (X = P, As and Bi), respectively. Therefore, an ioniccovalent mixture characterizes chemical bonds in the three compounds. Young's modulus *E* increases as we go from *PrBi* to *PrAs* to *PrP*. This confirms that *PrP* is stiffer than other two compounds. In addition, shear modulus increases as we go from PrBi to PrAs to PrP implying that PrBi is softer than the other two compounds. The calculated values of the B/G ratios are 1.51. 1.57 and 1.59 for PrP, PrAs and PrBi, respectively indicating that the three compounds are brittle. To obtain a deeper insight into thermal properties of PrX family, Debye temperature θ_D is calculated and found to be higher than that of the constituent Pr atom. Additionally, melting temperatures are significantly higher than that of consistent Pr atom. The elastic anisotropy of all compounds is calculated and subsequently, Young's modulus is estimated and plotted in a 3D stereogram. This study paves the way and motivates the experimentalists to design and fabricate PrX compounds as potential candidates for modern devices.

Declaration of Competing Interest

The authors declare that they have no known competing financial interests or personal relationships that could have appeared to influence the work reported in this paper.

Acknowledgements

The authors (T. Ghellab, Z. Charifi, and H. Baaziz) would like to thank the general directorate for scientific research and technological development for their financial support during the realization of this work.

References

- F. Hülliger, in: K.A. Gschneidner Jr., L. Eyring (Eds.), Handbook on the Physics and Chemistry of Rare Earths, vol. 4, Amsterdam, North-Holland, 1979, pp. 153.
- [2] C.G. Duan, R.F. Sabirianov, W.N. Mei, P.A. Dowben, S.S. Jaswal, E.Y. Tsymbal, J. Phys.: Condens. Matter 19 (2007) 315220.
- [3] L. Petit, R. Tyer, Z. Szotek, W.M. Temmerman, A. Svane, New J. Phys. 12 (2010) 113041.
- [4] S. Singh, K. Aneesh, R.K. Singh, J. Phys, Conf. Ser. 215 (2010) 012112.
- [5] G. Vaitheeswaran, L. Petit, A. Svane, V. Kanchana, M. Rajagopalan, J. Phys.: Condens. Matter 16 (2004) 4429.
- [6] M. De, P.K. Sinharoy, S.K. De, Phys. Lett. A 249 (1998) 147.
- [7] P. Soni, G. Pagare, V. Srivastava, S.P. Sanyal, Phase Transitions 82 (2009) 519–530.
- [8] P.K. Jha, S.P. Sanyal, Phys. Status Solidi B 205 (1998) 465.
- [9] S.J. Allen, D. Brehmer, C.J. Palmstrom, in: G.S. Pomrenka, P.B. Klein, D.W. Langer (Eds), Pittsburg, P.A., Materials Research Society, vol. 301, 1993, pp. 307.

- [10] I. Shirotani, J. Hayashi, K. Yamanashi, K. Hirano, T. Adachi, N. Ishimatsu, O. Shimomura, T. Kikegawa, Phys. B 334 (2003) 167.
- [11] I. Shirotani, K. Yamanashi, J. Hayashi, Y. Tanaka, N. Ishimatsu, O. Shimomura, T. Kikegawa, Solid State Commun. 127 (2003) 573–576.
- [12] I. Shirotani, K. Yamanashi, J. Hayashi, Y. Tanaka, N. Ishimatsu, O. Shimomura, T. Kikegawa, J. Phys.: Condens. Matter 13 (2001) 1939–1946.
- [13] T. Adachi, I. Shirotani, J. Hayashi, O. Shimomura, Phys. Lett. A 250 (1998) 389–393.
- [14] A. Chatterjee, A.K. Singh, A. Jayaraman, Phys. Rev. B 6 (1972) 2285
- [15] A. Jayaraman, in: K.A. Gschneidner Jr., L. Eyring (Eds.), Hand book on the Physics and Chemistry of Rare Earths, vol. 1, North-Holland, Amsterdam, 1979, pp. 9.
- [16] G. Pagare, V. Srivastra, Sankar P. Sanyal, R.K. Singh, Phys. Status Solidi B 241 (14) (2004) 3193.
- [17] B. Kocak, Y.O. Ciftci, K. Colakoglu, E. Deligoz, Comput. Mater. Sci. 50 (2011) 1958.
- [18] P. Blaha, K. Schwarz, G.H.K. Madsen, D. Kvasnicka, J. Luitz, K. Schwarz, Techn. Universitat Wien, Wien, 2008.
- 19] J.P. Perdew, K. Burke, M. Ernzerhof, Phys. Rev. Lett. 77 (1996) 3865.
- [20] H.J. Monkhorst, J.D. Pack, Phys. Rev. B 13 (1976) 5188.
- [21] A.D. Becke, E.R. Johson, J. Chem. Phys. 124 (2006) 221101.
- [22] J.F. Janak, Phys. Rev. B 18 (1978) 7165.
- [23] J.P. Perdew, R.G. Parr, M. Levy, J.M. Balduz, Phys. Rev. Lett. 49 (1982) 1691.
- [24] J.P. Perdew, M. Levy, Phys. Rev. Lett. 51 (1983) 1884.
- [25] L.J. Sham, M. Schlüter, Phys. Rev. Lett. 51 (1983) 1888.
- [26] V.I. Anisimov, J. Zaanen, O.K. Andersen, Phys. Rev. B 44 (1991) 943.
- [27] O. Gunnarsson, O.K. Andersen, O. Jepsen, J. Zaanen, Phys. Rev. B 39 (1989) 1708.
- [28] J.C. Slater, New York, McGraw-Hill, 1974.
- [29] G.K.H. Madsen, P. Novak, Euro. Phys Lett. 69 (2005) 777.
- [30] F.D. Murnaghan, Proc. Natl. Acad. Sci. USA 30 (1994) 5390.
- [31] B. Kocak, Y.O. Ciftci, K. Colakoglu, E. Deligoz, Phys. B 407 (2012) 316–323.
- [32] M.A. Blanco, A.M. Pendas, E. Francisco, J.M. Recio, R. Franko, J. Mol. Struct. (Theo-chem) 368 (1996) 245.
- [33] B. Kocaka, Y.O. Ciftcia, K. Colakoglua, E. Deligozb, Int. J. Mater. Res. 104 (2013) 99–108.
- [34] G. Pagare, S.P. Sanyal, Phase Transitions 79 (2006) 935.
- [35] T. Ghellab, Z. Charifi, H. Baaziz, Ş. Uğur, G. Uğur, F. Soyalp, Phys. Scr. 91 (2016) 045804.
- [36] T. Ghellab, Z. Charifi, H. Baaziz, K. Bouferrache, B. Hamad, Int. J. Energy Res. 43 (8) (2019) 3653–3667.
- [37] M. Des, P.K. Sinharoy, S.K. De, Phys. Lett. A 249 (1998) 147-152.
- [38] J. Mehl, Phys. Rev. B 47 (1993) 2493.
- [39] O.H. Nielsen, R.M. Martin, Phys. Rev. Lett. 50 (1983) 697.
- [40] Y. Le Page, P. Saxe, Phys. Rev. B 65 (2002) 104104.
- [41] S.Q. Wang, H.Q. Ye, Phys. Status Solidi B 240 (2003) 45.
- [42] C. Hua, Z. Zeng, L. Zhang, X. Chen, L. Cai, Phys. Condensed Matt. B 406 (2011) 669.
- [43] A. Love, Treatise on the Mathematical Theory of Elasticity, Cambridge University Press, Cambridge, 1944.
- [44] B. Mayer, H. Anton, E. Bott, M. Methfessel, J. Sticht, P.C. Schmidt, Intermetallics 11 (2003) 23.
- [45] W. Voigt, LehrbuchderKristallphysik, B.G. Teubner, Leipzig, Berlin, (1928).
- [46] A. Reuss, Berechnung der Fließgrenze, von Mischkristallen auf, Grund derPlastizitätsbedingungfürEinkristalle, Z. fürAngew. Math. und Mech. 9 (1) (1929) 49–58.
- [47] R. Hill, The elastic behavior of a crystalline aggregate, Proc. Phys. Soc. A 65 (1952) 349.
- [48] H. Fu, D. Li, F. Peng, T. Gao, X. Cheng, Comput. Mater. Sci. 44 (2008) 774.
- [49] A.F. Young, C. Sanloup, E. Gregoryanz, S. Scandolo, R.E. Hemley, H.K. Mao, Phys. Rev. Lett. 96 (2006) 155501.
- [50] J.R. Christman, Fundamentals of Solid State Physics, John Wiley & Sons, New York, 1988.
- [51] O.L. Anderson, J. Phys. Chem. Solids 24 (1963) 909.
- [52] E. Schreiber, O.L. Anderson, N. Soga: McGraw-Hill, New York, 1973.
- [53] T. Ghellab, H. Baaziz, Z. Charifi, K. Bouferrache, M.A. Saeed, A. Telfah, Mater. Res. Express 6 (2019) 075906.
- [54] T. Ghellab, H. Baaziz, Z. Charifi, K. Bouferrache, Ş. Uğur, G. Uğur, H. Ünver, Int. J. Modern Phys. B 33 (2019) 1950234.
- [55] P. Ravindran, L. Fast, P.A. Korzhavyi, B. Johansson, J. Appl. Phys. 84 (1998) 4891–4904.
- [56] S.I. Ranganathan, M. Ostoja-Starzewski, Phys. Rev. Lett. 101 (2008) 55504.
- [57] J.F. Nye, Oxford University Press, New York, 1985.